

The complex structure of the Mg II $\lambda\lambda$ 2795.523, 2802.698 Å regions of 64 Be stars

Evaggelia LYRATZI

*University of Athens, Faculty of Physics Department of Astrophysics, Astronomy and Mechanics
Panepistimioupoli, Zographou 157 84, Athens, Greece
elyratzi@phys.uoa.gr*

Emmanouel DANEZIS

*University of Athens, Faculty of Physics Department of Astrophysics, Astronomy and Mechanics
Panepistimioupoli, Zographou 157 84, Athens, Greece
edanezis@phys.uoa.gr*

Luka Č. POPOVIĆ

*Astronomical Observatory of Belgrade, Volgina 7, 11160 Belgrade, Serbia
Isaac Newton Institute of Chile, Yugoslavia Branch
lpopovic@aob.bg.ac.yu*

Milan S. DIMITRIJEVIĆ

*Astronomical Observatory of Belgrade, Volgina 7, 11160 Belgrade, Serbia
Isaac Newton Institute of Chile, Yugoslavia Branch
mdimitrijevic@aob.bg.ac.yu*

Dimitris NIKOLAIDIS

*University of Athens, Faculty of Physics Department of Astrophysics, Astronomy and Mechanics
Panepistimioupoli, Zographou 157 84, Athens, Greece
and*

Antonis ANTONIOU

*University of Athens, Faculty of Physics Department of Astrophysics, Astronomy and Mechanics
Panepistimioupoli, Zographou 157 84, Athens, Greece
ananton@phys.uoa.gr*

(Received 2000 December 31; accepted 2001 January 1)

Abstract

Here is studied the presence of absorption components shifted to the violet or the red side of the main spectral line (satellite, or discrete absorption components, i.e. SACs or DACs), in Mg II resonance lines' regions in Be stars and their kinematical characteristics. Namely our objective is to check if exists a common physical structure for the atmospheric regions creating SACs or DACs of the Mg II resonance lines. In order to do this, a statistical study of the Mg II $\lambda\lambda$ 2792.523, 2802.698 Å lines in the spectra of 64 Be stars of all spectral subtypes and luminosity classes is performed. We found that the absorption atmospheric regions where the Mg II resonance lines originated may be formed of several independent density layers of matter which rotate with different velocities. It is attempted also to separate SACs and DACs according to low or high radial velocity. The emission lines were detected only in the earliest and latest spectral subtypes.

Key words: Stars: atmospheres, early type, emission-line, Be, kinematics

1. Introduction

The Mg II resonance lines have a peculiar profile in the Be stellar spectra which indicates multicomponent nature of their origin region. Many researchers have observed the existence of absorption components shifted to the violet or the red side of the main spectral line (Underhill 1970; Marlborough, Snow, & Slettebak 1978; Dachs 1980; Doazan 1982; Danezis 1984; Danezis 1987; Danezis, Theodossiou, & Laskarides 1991; Sahade, Brandi, & Fontela 1984; Sahade & Brandi 1985; Hutsemékers 1985; Doazan et al. 1991; Laskarides, Danezis, & Theodossiou

1992; Cidale 1998; Lyratzi et al. 2003). These components, so called Discrete Absorption Components – DACs (Bates & Halliwell 1986) or Satellite Absorption Components – SACs (Danezis et al. 2003; Lyratzi & Danezis 2004), probably originate in separated regions which have different rotational and radial velocities. Especially in the case of very narrow DACs and SACs, they cannot be photospheric, but rather they have circumstellar or interstellar origin (Slettebak & Snow 1978). For example, Kondo, Morgan, & Modisette (1976) found that the shell absorption gets stronger from intermediate to the late B stars and suggested that “it might be

due to the rising temperature in the gaseous shell which converts Mg II to Mg III and to the weakening of the outward-driving mechanisms of the atmosphere". In any case, the whole feature of the Mg II resonance lines is not the result of a uniform atmospherical region, but the components are created in different regions, which rotate and move radially with different velocities. As de Jager et al. (1979) proposed in their study of 33 stellar spectra of all the spectral types, in the late B supergiants variable mass loss occurs, due to "occasional stellar "puffs" superposed on a more or less regular wind". They proposed that "there are concentrations of low-ionization species in the stellar wind as a result of the occurrence of significant density variations". Also, in order to explain the complex profiles of the Mg II resonance lines, Cidale (1998) proposed that the Be stellar atmospheres are composed from a classical photosphere, an extending high temperature chromosphere and a cool envelope. There is a question about contribution of different atmospherical layers, especially in the case of SACs and/or DACs phenomena, in the construction of the Mg II resonance lines' profiles.

The aim of this work is to statistically investigate the presence of SACs and/or DACs in Mg II resonance lines' regions in Be stars and their kinematical characteristics. Also, we would like to conclude about the limits of the rotational and radial velocities (V_{rot} , V_{rad}), as well as to check whether there exists a common physical structure for the atmospherical regions which create the Satellite Absorption Components (SACs) of the Mg II resonance lines in the spectra of all the Be stars. To do that, a statistical study of the UV Mg II resonance lines $\lambda\lambda$ 2795.523, 2802.698 Å in the spectra of 64 Be stars (all the spectral subtypes and luminosity classes) has been performed. The study is based on the model proposed by Danezis et al. (2003) and Lyratzi & Danezis (2004).

We decided to study the Mg II resonance lines, as they are characteristic of the cool envelope in Be stellar atmospheres, they are very intense features in the spectra of Be stars and they mostly present a complex and peculiar structure. Besides, since they are resonance lines, they give us a possibility to test the validity of the proposed model, as we have to adhere to all the necessary physical criteria and techniques (Danezis et al. 2003). Our purpose here was to study spectral lines which are created in cool regions (Mg II) in Be stellar atmospheres. Danezis (1987); Sahade, Brandi, & Fontela (1984); Sahade & Brandi (1985) detected multistructure in the regions where Fe II lines (I.P.=7.870 eV) are created in the spectra of Be stars which are characterized as iron stars. One of our purposes was to investigate whether the multistructure appears only in the Fe II spectral lines or in other spectral lines also with similar Ionization Potential, as Mg II (I.P.=7.646 eV). This is another reason why we chose to study the Mg II resonance lines and not some other resonance lines of the cool envelope, as N II (I.P.=14.490 eV), C II (I.P.=11.260 eV), Si II (I.P.=8.110 eV) or Al II (I.P.=5.986 eV). The study of Mg II resonance lines, gives us information not only about the cool envelope, but also for the multistructure of another ion that lies in the same

region where the Fe II spectral lines are created.

In §2 we describe the method of analysis, in §3 the observational data, in §4 the results and their discussion is given and in §5 we give our conclusions.

2. Method of spectral line analysis

Before starting with the description of the method used in our study, let us explain the differences between DACs and SACs. The DACs are components of a spectral line of a specific ion, shifted at different $\Delta\lambda$ from the transition wavelength of a line, because they are created in different density regions which rotate and move radially with different velocities (Lyratzi & Danezis 2004). The DACs are discrete lines, easily observed, in the spectra of some Be stars of luminosity class III, in the case of the Mg II doublet. However, if the layers that give rise to such lines rotate with quite large velocities and move radially with small velocities, then the produced lines are quite broadened and slightly shifted. As a result, they are blended among themselves as well as with the main spectral component and thus they do not appear as discrete, consequently they cannot be resolved. In such a case the name Discrete Absorption Component is inappropriate. Besides, as Peton (1974) first pointed out, these components appear as "satellites" in the violet or in the red side of the main spectral line's component as a function of the time or the phase in the case of a binary system. For these two reasons and in order to include all these lines that are components of the line profile either they are discrete or not to a unique name, it has been proposed (Lyratzi & Danezis 2004) that they should be named Satellite Absorption Components (SACs) as a general expression, because the Discrete Absorption Components are "Satellites" of a main spectral line, while the Satellite Absorption Components are not always discrete and cannot be easily resolved.

An additional peculiar phenomenon is that not all the lines of a specific ion have DACs. The DACs phenomenon is not a general one, but it is present in the case of some lines which have low excitation potential. For example, while the Mg II resonance lines at 2795.523, 2802.698 Å (multiplet 1) have DACs in the spectra of some Be stars, their subordinate lines at 2790.768, 2797.989 Å (multiplet 3) do not present the same phenomenon. Therefore, we decided to study the Mg II resonance lines, as they are the only Mg II doublet having DACs.

In order to try to obtain a qualitative picture we will use as an approximation the spherical geometry. According to it, there are two possibilities (see Fig. 1).

A) The region which creates the SACs or DACs may be an envelope around and near the rapidly rotating star. In such a case, the spherical model could give only a rough approximation but allow however to obtain some qualitative results. We note that such assumption is valid for some earlier models like e.g. Doazan and Thomas (1982) which can not explain the observed free-free emission or polarization, but we are interested here only in kinematic characteristics. In this case the calculated values of the

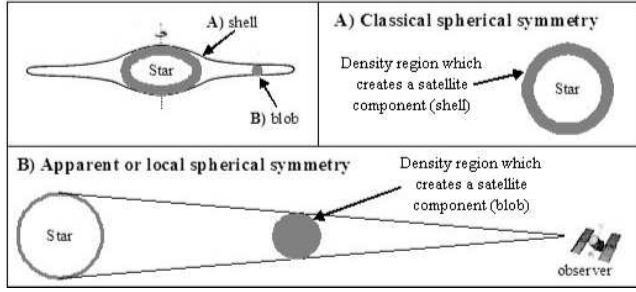


Fig. 1. Density regions which create the observed SACs or DACs in the stellar spectra.

radial velocity correspond to the component of the expansion or contraction velocity of the shell, which is projected to the observational axis.

B) The region which creates the SACs or DACs may be an independent density region (blob), which is spherically symmetric around its own center. Such density regions have been observed around stars that eject mass. In (Fig. 2) we see this phenomenon in WR 104, observed by Tuthill, Monnier & Danchi (1999). Such a region may be the one, which creates the Mg II resonance lines and which lies in the cool envelope of the stellar atmosphere. Such a blob may have three different motions: a) it may rotate around the star, b) it may expand or contract and c) it may move radially. This means that the calculated values of the radial velocity consist of three different components: a) the component of the rotational velocity of the blob around the star, projected to the observational axis, b) the component of the expansion or contraction velocity of the blob, projected to the observational axis and c) the component of the velocity of the blob's radial motion, projected to the line of sight.

In principle, as it is known, the star ejects mass with a specific radial velocity. The stream of matter is twisted, forming density regions such as interaction of fast and slow wind components, corrotating interaction regions (CIRs), structures due to magnetic fields or spiral streams as a result of the stellar rotation (Underhill & Fahey 1984; Mullan 1984a; Mullan 1984b; Mullan 1986; Prinja & Howarth 1988; Cranmer & Owocki 1996; Fullerton et al. 1997; Kaper et al. 1996; Kaper et al. 1997; Kaper et al. 1999; Cranmer, Smith, & Robinson 2000). Consequently, hydrodynamic and magnetic forces act as centripetal forces, resulting that the outward moving matter twists and moves around the star (see Fig. 2). This motion of the matter is responsible for the formation of high density regions (shells, blobs, puffs, spiral streams), which, either they are spherically symmetric with respect to the star or with respect to their own center (Danezis et al. 2003; Lyrtzi & Danezis 2004) (see Fig. 1).

In order to study the physical structure and the existence of SACs phenomena in the regions where these lines are created we used the model proposed by Danezis et al. (2003) and Lyrtzi & Danezis (2004). This model allows us to calculate the rotational (V_{rot}) and radial velocities (V_{rad}) of independent density layers of matter in these

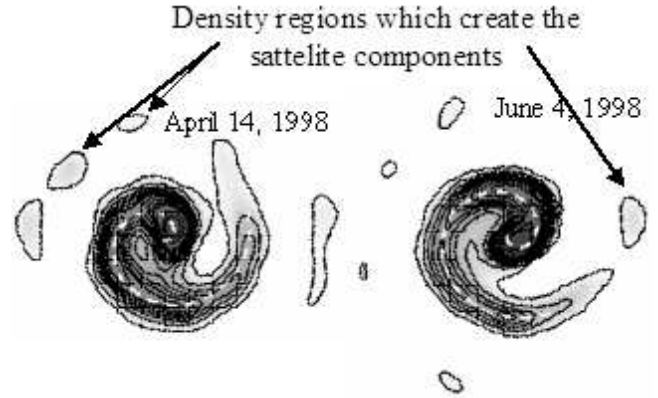


Fig. 2. Due to the rotation of the star the ejected matter forms spiral streams which produce blobs that create the observed SACs or DACs in the stellar spectra. This figure is taken from Tuthill, Monnier & Danchi (1999)

regions, as well as the optical depth (τ) and the column density (n). If the considered SACs or DACs originate from "puffs" or "blobs" created by stellar winds in a cool extended envelope, the real shape of the envelope is not crucial. If the considered features are created in the envelope's layers we also could obtain some qualitative conclusions, since we are interested only in kinematical properties here. Moreover, there is no a sophisticated or rough model of Be star which could fit the observed profiles considering their complex structure so that there is no results of similar investigations for comparisons.

Let us consider that the area of gas, which creates a specific spectral line, consists of i independent absorbing density regions followed by j independent regions that both absorb and emit and an outer absorbing region. Such a structure produces DACs or SACs in the observed spectra (Danezis et al. 2003) and the final line function which can describe the complex line profiles of the observed spectral lines is (Danezis et al. 2003; Lyrtzi & Danezis 2004):

$$F_{\lambda} = [F_{\lambda 0} \prod_i e^{-L_i \xi_i} + \sum_j S_{\lambda e j} (1 - e^{-L_{e j} \xi_{e j}})] e^{-L_g \xi_g}$$

where F_{λ} is the observed flux, $F_{\lambda 0}$ is the initial flux, $S_{\lambda e j}$ are the source functions of each emitting density region, ξ is the optical depth in the center of the line and L_i , $L_{e j}$, L_g are the distribution functions of the absorption coefficients $k_{\lambda i}$, $k_{\lambda e j}$, $k_{\lambda g}$, respectively. Each L depends on the values of the rotational and the radial velocity of the density region, which forms each component of the spectral line (V_{rot} , V_{rad}) (Danezis et al. 2003; Lyrtzi & Danezis 2004). The product of L and ξ is the optical depth of each region.

This function does not depend on the geometry of the regions creating the observed feature. The considered geometry of the regions is taken into account in order to define the distribution function L . This means that L may represent any distribution which considers certain geometry (see Appendix A), without changing anything in F_{λ} .

Each component of the spectral line, which is formed by

the i^{th} density region of matter, must be accurately reproduced by the function $e^{-L_i \xi_i}$ by applying the appropriate values of V_{rot_i} , V_{rad_i} and ξ_i . Using the best model's fit for a complex spectral line, we can calculate the apparent radial and rotational velocity (V_{rad_i}, V_{rot_i}) and the optical depth (ξ_i) in the center of the line of the region in which the main spectral line and its SACs are created.

In the case that we want to consider that some other physical parameters are responsible for the line broadening and not the rotation of the region which produces the studied spectral lines, we may replace the exponential $e^{-L\xi}$ with another classical distribution.

In the case of emission lines, each emission component, which is formed by the j^{th} density region of matter, must be accurately reproduced by the function $S_{\lambda_{ej}}(1 - e^{-L_{ej}\xi_{ej}})$, by applying the appropriate values of V_{rot_i} , V_{rad_i} , ξ_i and S . Using the best model's fit for a complex spectral line, we can calculate the apparent radial and rotational velocity (V_{rad_i}, V_{rot_i}), the optical depth (ξ_i) in the center of the line and the source function S of the region in which the emission component is created.

The proposed model is relatively simple, aiming to describe the regions where the spectral lines which present SACs are created. With this model we study the regions of a specific ion which creates a specific spectral line.

This model presupposes that the main reason of the line broadening is the rotation of the region that gives rise to the spectral line (Doazan 1982). We can accept this assumption when we deal with the inner layers to the post-coronal regions. Thus, for these atmospheric layers the model gives satisfactory results.

3. Observational data and fitting procedure

The data we used are the Mg II resonance lines of 64 Be stars taken from the IUE Archive Search database¹. The stellar spectra were observed with IUE satellite using the Long Wavelength range Prime and Redundant cameras (LWP, LWR) at high resolution (0.1 to 0.3 Å). In Table 1 we give the list of stars, their spectral type and the type of camera used during observations.

Our first step is to identify the spectral lines in the studied wavelength range, in order to find out which lines may be blended with the Mg II doublet and, thus, may contribute to the observed features. The identification has been made by NIST Atomic Spectra Database², as well as the catalogues of Moore (1968) and Kelly (1979). In this specific spectral range the adjacent features of the Mg II profiles are intense, but they are away from the Mg II spectral features, so that, in spite of their important influence on the wings, their much smaller influence in central parts is not important for our discussion. Moreover, as we deal with resonance lines, we know that if one line of the doublet is well fitted, we should apply the same parameters to the other one, even if the fit is not so good. In this case the unfitted regions correspond to blends. Also,

the level of continuum is calculated for the whole spectrum taken by IUE. This means that its suppression by the blends does not affect our calculations.

The procedure that we followed for the decomposition of the lines is described in Danezis et al. (2003). The way, the criteria and discussion about the model we use to fit the observed spectral lines are presented in Danezis et al. (2003) and they are explained in more detail in Lyratzi & Danezis (2004) and an application of the method is given in Popović et al. (2004). This means that we tried to fit the observed profiles of the Mg II resonance lines with the less possible components. At first we tried to fit the observed spectral feature with one component. If this had not been possible, we added one more component and then another, until we accomplished the best fit with the less possible components. This means that we fitted the observed Mg II features with one to four components, for different stars. Our results are shown in Tables 2 and 3.

¹ <http://archive.stsci.edu/cgi-bin/iue>

² http://physics.nist.gov/cgi-bin/AtData/lines_form

Table 1. The list of Be stars with spectral type (columns 2, 5) and the type of the camera used during the observations (columns 3, 6).

Star	Spectral Type	Camera	ref	Star	Spectral Type	Camera	ref
HD 5394	B0 IV : evar	Lwr 07861	1	HD 25940	B3 V e	Lwr 05950	2
HD 53367*	B0 IV : e	Lwr 09286	1	HD 45725*	B3 V e	Lwp 10041	2
HD 203374**	B0 IV pe	Lwp 07400	1	HD 183362	B3 V e	Lwp 11044	2
HD 206773	B0 V : pe	Lwr 14808	1	HD 208057	B3 V e	Lwp 29221	2
HD 200310	B1 V e	Lwr 09544	1	HD 205637	B3 V : p	Lwr 05947	4
HD 212571	B1 V e	Lwr 05948	2	HD 217543	B3 V pe	Lwp 13326	2
HD 44458*	B1 V pe	Lwp 30173	1	HD 217050**	B4 III pe	Lwr 05933	2
HD 200120	B1.5 V nne	Lwr 11035	2	HD 89884	B5 III	Lwp 29529	6
HD 193237	B2 pe	Lwr 07990	2	HD 22192	B5 V e	Lwr 06898	2
HD 45910*	B2 III e	Lwr 12138	3	HD 23302	B6 III e	Lwr 09071	2
HD 37202	B2 IV p	Lwr 05888	4	HD 45542	B6 III e	Lwp 07631	2
HD 36576	B2 IV - V e	Lwp 14029	2	HD 109387	B6 III pe	Lwr 04132	2
HD 212076	B2 IV - V e	Lwr 03406	2	HD 23480	B6 IV e	Lwr 05219	2
HD 32991*	B2 V e	Lwr 11426	2	HD 217891	B6 V e	Lwr 09069	2
HD 58050	B2 V e	Lwr 14810	2	HD 138749	B6 V nne	Lwr 07858	2
HD 164284	B2 V e	Lwr 11038	2	HD 23630	B7 III	Lwr 09060	2
HD 41335	B2 V ne	Lwr 07384	2	HD 209409	B7 IV e	Lwp 15464	2
HD 52721	B2 V ne	Lwp 05462	5	HD 6811	B7 V e	Lwr 09070	7
HD 58343	B2 V ne	Lwr 07363	6	HD 192044*	B7 V e	Lwp 08135	8
HD 148184	B2 V ne	Lwr 06744	6	HD 210129	B7 V ne	Lwp 23173	7
HD 202904	B2 V e	Lwr 07343	2	HD 142983	B8 Ia/Iab	Lwr 07359	6
HD 65079	B2 V ne	Lwp 30119	5	HD 29866	B8 IV ne	Lwr 08745	2
HD 28497	B2 V ne	Lwr 07337	6	HD 47054	B8 V e	Lwp 13074	9
HD 45995*	B2 V nne	Lwr 08648	1	HD 183914*	B8 V e	Lwr 04609	9
HD 10516	B2 V pe	Lwr 07335	2	HD 50138	B8 V e	Lwr 09358	11
HD 187567*	B2.5 IV e	Lwp 14025	2	HD 58715	B8 V var	Lwp 10104	10
HD 191610	B2.5 V e	Lwr 07342	2	HD 23552**	B8 V ne	Lwr 08744	7
HD 32343*	B2.5 V e	Lwr 05890	2	HD 185037	B8 V ne	Lwp 08136	9
HD 65875	B2.5 V e	Lwr 05616	2	HD 199218	B8 V nne	Lwp 09903	7
HD 60855**	B2/B3 V	Lwp 15477	6	HD 91120	B8/B9 IV/V	Lwp 07475	6
HD 37490*	B3 III e	Lwr 07361	1	HD 142926	B9 pe	Lwr 05768	7
HD 50820	B3 IV e+...	Lwr 16776	2	HD 144	B9 III e	Lwr 08997	7

* Double system ** Triple system

References: (1) Morgan, Code & Whitford 1955; (2) Lesh 1968; (3) Sahade, Brandi & Fontela 1984; (4) Herbig & Spalding 1955; (5) Guetter 1968; (6) Houk N. & Smith-Moore 1988; (7) Cowley 1972; (8) Osawa 1959; (9) Cowley et al. 1969; (10) Slettebak 1954; (11) Houziaux & Andrillat 1976.

Table 2. The kinematical parameters for absorption regions for considered stars: the rotational (V_{rot}) and the radial (V_{rad}) velocities in km s^{-1} .

Star	Spectral Type	V_{rot1}	V_{rad1}	V_{rot2}	V_{rad2}	V_{rot3}	V_{rad3}	V_{rot4}	V_{rad4}
HD 5394	B0 IV evar	25	8.8	50	12.3				
HD 53367	B0 IV : e	24	-18.0	37	-12.0	71	-7.0		
HD 203374	B0 IV pe	24	4.5	36	3.5	60	2.0		
HD 206773	B0 V : pe	28	15.5	46	18.5				
HD 200310	B1 V e	25	10.1						
HD 212571	B1 V e	22	-2.5	40	-11.0				
HD 44458	B1 V pe	22	-17.5	37	-19.5	83	-29.0		
HD 200120	B1.5 V nne	28	-0.4						
HD 193237	B2 pe	30	-18.6	45	-18.1	86 (DAC)	-200.6	115 (DAC)	-200.1
HD 45910	B2 III e	24	13.0	42	11.0	60 (DAC)	-229.5	170 (DAC)	-182.0
HD 37202	B2 IV p	29	-18.0	48	-21.0			125	-33.0
HD 36576	B2 IV - V e	29	-43.0			80	-21.0		
HD 212076	B2 IV - V e	20	-1.0	34	-1.5				
HD 32991	B2 V e	19	-15.4	38	-21.9				
HD 58050	B2 V e	25	-35.9	49	-28.4				
HD 164284	B2 V e	28	13.3			63	33.8		
HD 41335	B2 V ne	22	-9.5	38	-1.5	80	27.0	100	40.0
HD 52721	B2 V ne	18	12.3	34	11.3	65	31.3		
HD 58343	B2 V ne	21	-1.8	50	-5.2				
HD 148184	B2 V ne	17	19.9	30	20.9				
HD 202904	B2 V e	20	4.0	31	4.5				
HD 65079	B2 V ne	29	8.0			74	-12.5		
HD 28497	B2 V ne	8	-45.0	37	-34.5	60	-35.0		
HD 45995	B2 V nne	29	-17.0	45	-20.0	69	-24.0		
HD 10516	B2 V pe	22	-1.0	37	-2.3	50	-5.8		
HD 187567	B2.5 IV e	19	23.6	32	24.6	50	26.1		
HD 32343	B2.5 V e	20	8.4			78	17.9		
HD 65875	B2.5 V e	17	14.0	35	18.0				
HD 191610	B2.5 V e	20	-45.6	45	-53.6				
HD 60855	B2/B3 V			45	-14.6	71	22.9	139	-29.6
HD 37490	B3 III e	20	-5.3	35	-8.3	54	-18.8	98	-10.3
HD 50820	B3 IV e+...	24	-13.0	50	-9.5				
HD 25940	B3 V e	22	0.7	42	-2.3				
HD 45725	B3 V e	18	-9.5	34	-10.5	65	-13.0		
HD 183362	B3 V e	24	24.2	34	24.2	68	19.7		
HD 208057	B3 V e	23	12.3			75	9.8		
HD 205637	B3 V : p	22	17.5	39	15.5			115	9.0
HD 217543	B3 V pe	26	16.5	51	15.5			130	23.5
HD 217050	B4 III pe	35	14.3	54	17.8	84	32.3		
HD 89884	B5 III			33	-9.5	60	1.5		
HD 22192	B5 V e	16	-2.0	32	-1.0	52	-7.0		
HD 23302	B6 III e	21	-9.9			86	-8.9		
HD 45542	B6 III e	15	-24.4	33	-24.9	58	-15.4		
HD 109387	B6 III pe	18	-11.4			66	-28.4		
HD 23480	B6 IV e	20	-7.7	32	0.3				
HD 217891	B6 V e	18	-0.8						
HD 138749	B6 V nne	27	22.5	47	14.5				
HD 23630	B7 III	20	-9.0	45	-9.0				
HD 209409	B7 IV e	21	-9.0	38	-9.0	83	-5.0		
HD 6811	B7 V e	19	3.3	35	1.8			169	12.8
HD 192044	B7 V e	25	19.5	52	8.5				
HD 210129	B7 V ne	21	62.6	52	43.1				
HD 142983	B8 Ia/Iab	21	-7.0	39	8.0	60	11.5	95	16.5
HD 29866	B8 IV ne	26	-42.0			85	41.5		
HD 47054	B8 V e	24	-30.0	42	-31.5				

Table 2. (Continued.)

HD 183914	B8 V e	17	16.8	37	20.8				
HD 50138	B8 V e	27	-36.0						
HD 58715	B8 V var	22	-21.5	44	-9.0				
HD 23552	B8 V ne			33	24.7				
HD 185037	B8 V ne	26	12.0	45	18.0				
HD 199218	B8 V nne	17	4.7	35	4.2			95	7.7
HD 91120	B8/B9 IV/V	23	-13.5	39	-15.0				
HD 142926	B9 pe	18	-12.9	50	2.1	67	7.6	165	3.6
HD 144	B9 III e	28	-30.6	53 (DAC)	-188.6	80 (DAC)	-187.1	178 (DAC)	-129.6

Table 3. The same as in Table 2, but for the emission component where it is present.

Star	Spectral Type	V_{rote}	V_{rade}
HD 203374	B0 IV pe	20	72
HD 45910	B2 III e	34	81
HD 32991	B2 V e	57	13
HD 164284	B2 V e	120	-1
HD 148184	B2 V ne	50	33
HD 45995	B2 V nne	46	102
HD 65875	B2.5 V e	30	53
HD 50820	B3 IV e+...	59	-87
HD 217891	B6 V e	50	6
HD 192044	B7 V e	94	7
HD 210129	B7 V ne	97	-29
HD 47054	B8 V e	81	0
HD 50138	B8 V e	53	120
HD 199218	B8 V nne	131	15

Table 4. Values of the confidence with which the accepted fit is better than the fit with the one less component.

Star	4-3 comps	3-2 comps	2-1 comps	Star	4-3 comps	3-2 comps	2-1 comps
HD 5394		0.9132		HD 25940		0.9972	
HD 53367	1.0000			HD 45725		1.0000	
HD 203374	0.9483			HD 183362	0.9807		
HD 206773		1.0000		HD 208057		1.0000	
HD 200310			0.9993	HD 205637	1.0000		
HD 212571		0.9826		HD 217543	1.0000		
HD 44458	0.9981			HD 217050	1.0000		
HD 200120			1.0000	HD 89884		1.0000	
HD 193237	1.0000			HD 22192		1.0000	
HD 45910	0.1609			HD 23302		1.0000	
HD 37202	1.0000			HD 45542		0.9998	
HD 36576		0.9931		HD 109387	0.9996		
HD 212076		1.0000		HD 23480		0.9998	
HD 32991		0.6737		HD 217891			
HD 58050		0.9978		HD 138749		0.9936	
HD 164284		0.7826		HD 23630		0.9986	
HD 41335	1.0000			HD 209409		0.9954	
HD 52721		0.9767		HD 6811	1.0000		
HD 58343		0.9928		HD 192044		0.8070	
HD 148184		0.9396		HD 210129		0.8927	
HD 202904		0.9475		HD 142983	1.0000		
HD 65079	1.0000			HD 29866		1.0000	
HD 28497	1.0000			HD 47054		0.9086	
HD 45995	0.1169			HD 183914		0.9975	
HD 10516	0.9981			HD 50138			0.6758
HD 187567		0.9747		HD 58715		0.9189	
HD 191610		0.9990		HD 23552			1.0000
HD 32343		0.7793		HD 185037		0.9500	
HD 65875		1.0000		HD 199218		0.9693	
HD 60855	0.9800			HD 91120		0.9778	
HD 37490	1.0000			HD 142926	1.0000		
HD 50820		0.6221		HD 144	1.0000		

In order to be certain that we have accomplished the best fit, we performed an F-test, between the fit that we accept as the best and a fit with one component less. We present the results of the F-test in Table 4, where we give the values of the confidence with which the accepted fit is better than the fit with the one component less. We did not perform an F-test between the best fit and a fit with one component more, as this last one fit presented extreme differences with the observed spectral line profiles or because the values of the measured parameters go against the classical theory for resonance lines (Danezis et al. 2003; Lyratzi & Danezis 2004).

4. Results and discussion

DACs phenomenon is quite common in O- and early B-type stars. However, we found that DACs phenomenon is also observed in late B-type stars (as in the case of HD 144). Moreover, many researchers (Underhill 1975; Morgan, Kondo, & Modisette 1977; Marlborough, Snow, & Slettebak 1978; de Jager et al. 1979; Doazan 1982; Sahade, Brandi, & Fontela 1984; Sahade & Brandi 1985; Hutsemékers 1985), even if they do not use the name DACs, observed the same phenomenon. We point out also, that in Underhill (1970); Marlborough, Snow, & Slettebak (1978); Dachs (1980); Doazan (1982); Sahade, Brandi, & Fontela (1984); Sahade & Brandi (1985); Hutsemékers (1985); Doazan et al. (1991); Cidale (1998) only the known DACs phenomenon was investigated. However, in the present paper the similar phenomenon of SACs is introduced and we investigate whether this phenomenon is able to explain the complex structure of Mg II resonance lines in the stellar spectra of all the Be spectral subtypes. Our result is that the SACs phenomenon is able to explain this complex structure.

Using the model described above we find the best fit for the Mg II resonance lines of 64 Be stars given in Table 1. In Fig. 3, we give the best fit of the Mg II resonance lines for two stars (HD 45910 and HD 41335). The first one (HD 45910) presents DACs, where the decomposition of the three different components is easy, while the second one (HD 41335) presents SACs, where, it is hard to decompose the three different components, without the convenient model. So, one can see that the model describes conveniently the Mg II complex profiles and the complex structure of the regions where these lines are created. In the studied IUE spectra, the interstellar lines are systematically shifted to the red for $+99 \pm 16 \text{ km s}^{-1}$. We used the Hipparcos catalogues³ and we applied the corrections for the systemic velocity of individual stars (Smith 2001) and for the orbital motion of the stars which are members of binary systems. Our results, shown in Tables 2 and 3 as well as in Figs. 4 - 8, are correspondingly corrected.

We should note that in our sample 15 binary and multiple systems are present (see Table 1). Considering that the origin of DACs and SACs, in principle might be different than in single stars, at the beginning we separately

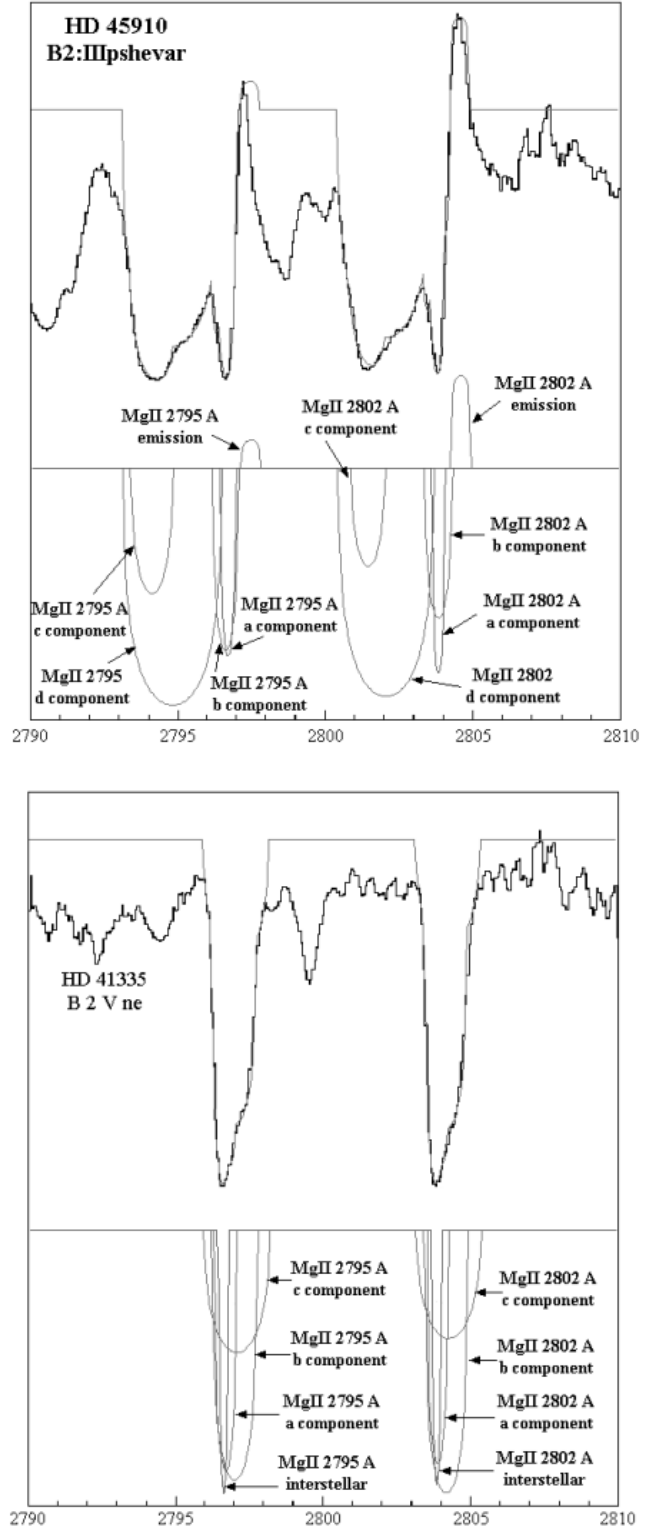


Fig. 3. The Mg II resonance line profiles fitted with the model for HD 45910 and HD 41335. The thick lines present observations, and the thin lines the best fit. The DACs (HD 45910) and SACs (HD 41335) are present below.

³ <http://vizier.u-strasbg.fr/viz-bin/VizieR-3>

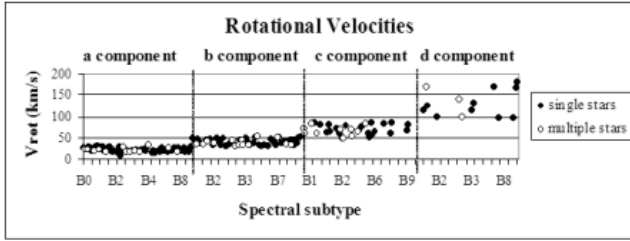


Fig. 4. Mean values for each spectral subtype of the rotational velocities of all the SACs as a function of the spectral subtype.

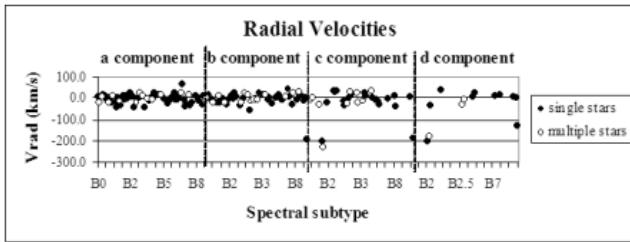


Fig. 5. Mean values for each spectral subtype of the radial velocities of all the SACs as a function of the spectral subtype.

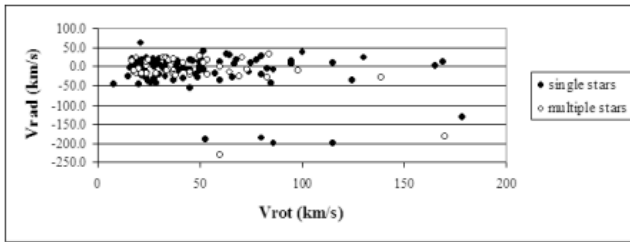


Fig. 6. Radial velocities of all the SACs as a function of the respective rotational velocities.

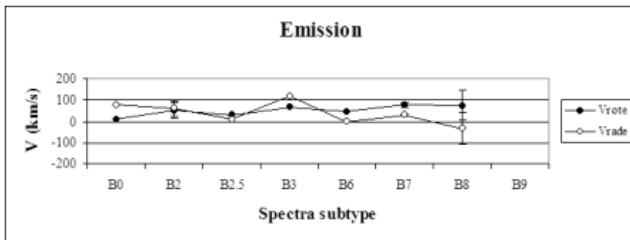


Fig. 7. Mean values for each spectral subtype of the rotational and radial velocities of the emission component as a function of the spectral subtype.

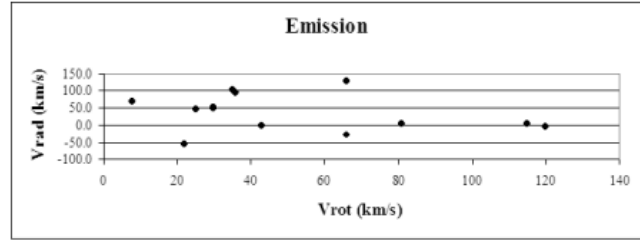


Fig. 8. Radial velocities of the emission component as a function of the respective rotational velocities.

analyzed this kind of stars (presented with open circles in Figs. 4 - 6). However, we found that there is no systematic difference between single and binary/multiple stars. Consequently, in further analysis we will not treat binary/multiple systems in a different way.

From the fit we obtained the rotational (V_{rot_i}) and radial velocities (V_{rad_i}) for each Mg II resonance line originating within the region.

In Tables 2 and 3 we present the kinematical parameters for the absorption Mg II resonance line forming regions (Table 2), as well as for the emission ones (Table 3). As one can see, not all the studied stars have an emission component, but only the ones listed in Table 3. One could assume that these emission components are the emission part of P Cygni profiles formed by scattering. In that case, their wavelength and width does not represent the radial and rotational velocity. This could explain the majority of positive radial velocities since in such a case even in outflowing wind, lines will be widened and red shifted. However, two cases with large negative radial velocities indicate that the real picture may be more complicated. We know that the disk models, in many cases, may produce theoretically only the shape of line profiles, but they are not able to fit them. So, in such cases, we may consider that the observed profile results from a different mechanism. In Table 2 we give the list of stars, their spectral subtype (columns 1 and 2, respectively) and the values of the rotational velocities (columns 3, 5, 7 and 9) and the radial velocities (columns 4, 6, 8 and 10) of the respective components. Also, in Table 3, we present the kinematical parameters of the emission components. In column 1 we present the list of stars, in column 2 their spectral subtype and in columns 3 and 4 the values of the rotational and the radial velocity, respectively. Let us point out, here, that the calculated values correspond to the regions which create the SACs or DACs. Especially, the obtained rotational velocities correspond to the rotation of the region around itself and not around the star.

In Figs. 4 and 5 we present, separately, the rotational velocities and the radial velocities, respectively, of all the SACs as a function of the spectral subtype. In Fig. 5 the radial velocity's values which correspond to the DACs are clearly seen. In Fig. 6 we present the radial velocities of all the SACs as a function of the respective rotational velocities. In Fig. 7 we present the rotational and radial velocities' mean values of the two resonance lines of the

emission component as a function of the spectral subtype. Each point refers to the mean value extracted for each spectral subtype. Finally, the radial velocities of the emission component as a function of the respective rotational velocities are given in Fig. 8.

The values we have calculated lie within a small range and we can obtain only the mean values of radial and rotational velocities and their standard deviation. The points in the diagrams correspond to the mean values of the velocities for each spectral subtype and the error-bars which appear in some of the diagrams to the standard deviation. This standard deviation is not only a statistical error but it includes also the possible variation of the inclination axis and the error of the spectral classification, as the spectral classification which was based in the optical range could not be appropriate for the UV range. This means that the error-bars which appear in the diagrams include the statistical error as well as the dispersion of the values due to the different axis inclination.

The reproduction of the Mg II resonance lines $\lambda\lambda$ 2795.523, 2802.698 Å using the model where SACs are present, suggests that the atmospheric regions, where the Mg II doublet is created, may be described in a unique way for all the studied Be stars. This result confirms the suggestion given by de Jager et al. (1979) that in Be stellar atmospheres exists a concentration of low-ionization species in the stellar wind and it is due to the occurrence of significant density variations. This result is also in agreement with the results of Morgan, Kondo, & Modisette (1977), who proposed that there are “significant absorption features” on the left side of each resonance line, which are attributed to “additional absorption within the stellar extended atmosphere”. These “significant absorption features” can be the SACs that appear in the spectra of the early type stars. Danezis et al. (2003) and Lyratzi & Danezis (2004) suggested that the peculiar phenomena observed in the spectra of Oe and Be stars, such as the SACs, are due to independent density regions in the stellar environment. Such regions may be structures that cover all or a significant part of the stellar disk (shells, blobs, puffs, bubbles) (Underhill 1975; de Jager et al. 1979; Henrichs 1984; Underhill & Fahey 1984; Bates & Halliwell 1986; Grady et al. 1987; Lamers, Faraggiana, & Burger 1980; Waldron, Klein & Altner 1992; Cranmer & Owocki 1996; Rivinius et al. 1997; Kaper et al. 1996; Kaper et al. 1997; Kaper et al. 1999; Markova 2000), interaction of fast and slow wind components, CIRs, structures due to magnetic fields or spiral streams as a result of the stellar rotation (Underhill & Fahey 1984; Mullan 1984a; Mullan 1984b; Mullan 1986; Prinja & Howarth 1988; Cranmer & Owocki 1996; Fullerton et al. 1997; Kaper et al. 1996; Kaper et al. 1997; Kaper et al. 1999; Cranmer, Smith, & Robinson 2000). This is the common theory which explains the DACs phenomenon in early type stars. We have found DACs phenomena in early B-type stars (e.g HD 45910), as well as in late B-type stars (e.g. HD 144).

As one can see from Table 2, the SACs phenomenon appears to be a classical one for the Be stars. In Fig. 3 and

in Table 2 one can see that all the studied stars present discernible (DACs) or indiscernible (SACs) components of the Mg II resonance lines. The indiscernible components appear in the spectra of all the stars of luminosity classes IV and V and most of the stars of luminosity class III. It is very interesting that the SACs are observed as discrete lines (DACs) in the spectra of the three stars HD 193237 (B2 pe), HD 45910 (B2 III e) and HD 144 (B9 III e), because they present quite different radial shifts. This means that the regions which create these lines move radially with relatively large velocities producing lines shifted enough to be easily observed in the spectra. On the other hand, in the case of all the rest studied stars, the SACs of the Mg II resonance lines present similar radial velocities, resulting to the SACs being blended among themselves. In this case, we can distinguish these lines by the systematic differentiations of the rotational velocities.

The decomposition of the observed profiles for the Mg II regions in Be stellar atmospheres confirms the existence of independent density regions, since by using such a structure, we were able to reproduce the resonance lines of Mg II in all the studied stars. This decomposition is physically meaningful as it enables us to detect kinematically different regions with different rotational and radial velocities, as well as the optical depth and the column density, for each of the Mg II independent density regions, which produce DACs or SACs.

Our analysis shows that regions where the considered Mg II resonance lines originate (“blobs” and “puffs” created by winds or cool extended envelopes) may consist of more independent density layers of matter with different kinematical properties (one to four in the analyzed cases). We identified them by the decomposition of observed Mg II lines in the number of components which fit best the observed profile. Namely, depending on particular star, we obtain that SACs or DACs may be divided in several rotational velocity groups (average values for rotational velocity groups found to be present at 64 considered stars are 22 ± 5 km s⁻¹, 41 ± 7 km s⁻¹, 69 ± 11 km s⁻¹ and 130 ± 31 km s⁻¹). The corresponding radial velocities are near zero (-3.3 ± 20.3 km s⁻¹ - for the first density region; -3.6 ± 20.6 km s⁻¹ - for the second; -1.0 ± 21.8 km s⁻¹ - for the third one and $+4.0\pm 22.7$ km s⁻¹ for the fourth one). In the spectra of the stars HD 193237 (B2 pe), HD 45910 (B2 III e) and HD 144 (B9 III e) the SACs appear as discrete components (DACs) and the radial velocities of the third and the fourth density region are -205.7 ± 21.7 km s⁻¹ and -170.6 ± 36.6 km s⁻¹, respectively. In the case of the star HD 144, the second component appears also as a discrete component. The radial velocity of the region, which creates this component is -188.6 km s⁻¹ (Figs. 4, 5 and 6). The observed velocity dispersion may be due to the different values of the rotational axis inclination of the regions where the SACs are created. The results presented above confirm that the Mg II doublet is more or less stable for a given spectral type as Gurzadyan (1975) suggested. We did not find any variation of the velocities in the Mg II regions with the luminosity class, except in the case of the peculiar stellar spectra, where the SACs

appear as discrete lines (DACs), while Kondo, Morgan, & Modisette (1976) proposed that, apart from the difference among spectral subtypes, there is probably difference among luminosity classes too.

We assume that independent density regions corresponding to particular components of considered Mg II lines (one to four components corresponding to one to four regions in the case of 64 stars analyzed here), lie all in the cool stellar envelope. Depending on the temperature, different ions with different Ionization Potential are created in different regions at different distances from the star. This means that the spectral lines observed in the spectra of Be stars derive from specific atmospheric regions, different among themselves. The ions which are created very close to the star lie in regions which present spherical symmetry around the star (case A in Fig. 1). On the other hand, the ions which are created at long distance from the star lie in regions which present spherical symmetry around their own center and not around the star (case B in Fig. 1). As the ionization potential of the Mg II ions is $I.P.=7.646$ eV, the Mg II ions can be created only at great distance from the center of the star, meaning in the disk, where spherical symmetry around the star cannot be accepted. This means that the Mg II ions lie at regions which present topical or apparent spherical symmetry (case B in Fig. 1). As a result, the Mg II spectral lines and their SACs/DACs may derive only from such regions (case B in Fig. 1) and not from classically spherical regions around the star (case A in Fig. 1). This kind of density regions (blobs) have been proposed by many researchers (Underhill 1975; de Jager et al. 1979; Lamers, Faraggiana, & Burger 1980; Henrichs 1984; Underhill & Fahey 1984; Mullan 1984a; Mullan 1984b; Mullan 1986; Bates & Halliwell 1986; Grady et al. 1987; Prinja & Howarth 1988; Waldron, Klein & Altner 1992; Cranmer & Owocki 1996; Fullerton et al. 1997; Rivinius et al. 1997; Kaper et al. 1996; Kaper et al. 1997; Kaper et al. 1999; Markova 2000; Cranmer, Smith, & Robinson 2000) and are detected in many other cases, as in active stars (WR 104, see Fig. 2) and many quasars, as we observe DACs/SACs in their UV spectra (Danezis et al. 2006). This means that the density regions are a common phenomenon, observed in different levels. The fact that we found one to four components is accidental. In principle, there could be more or less. Although the number of components is different in different stars, we may conclude that the Mg II resonance lines forming regions present a complex structure.

Our proposition that SACs phenomenon is responsible for the structure of Mg II lines means that we expect theoretically that the Mg II components have similar radial velocities, within the range of statistical error (~ 10 km/s). The problem was how to distinguish them. The common idea (Doazan 1982) is that the radial velocity of the kinematically independent regions is a function of the distance from the rapidly rotating Be star. According to that, our first thought was to distinguish these regions according to their rotational velocities, which is confirmed by our calculations. Namely, the regions which create the Mg II

lines have similar radial velocities and different rotational velocities.

In our sample we cannot detect high radial velocities, whatever method we use (the proposed model or any other classical method). The radial velocities of all the SACs, in all the studied stars are about 0 km/s and only in the case of the stars HD 193237 (B2 pe), HD 45910 (B2 III e) and HD 144 (B9 III e), where we observe DACs, we calculated radial velocities with values between -130 km/s and -230 km/s. We can detect the same phenomenon in the case of Si IV in a sample of 68 Be stars (values of radial velocities between -116 km/s and +25 km/s) (Lyrtzi et al. 2006), as well as in the case of Ha in 120 Be stars (values of radial velocities around 0 km/s) (Lyrtzi et al. 2005). These results indicate that in the atmospheric layers from the photosphere (very broad components of Ha) to the cool envelope (Mg II resonance lines) we cannot detect very high radial velocities. However, as we expected, the presence of DACs in three stars of our sample indicate that from the regions near to the star towards the ones away from the star, the radial velocity increases, but it does not reach high values, as happens in the case of Oe stars. In the case of specific Be stars that present DACs with high radial velocities in some of their spectra, e.g. 59 Cyg and γ Cas (Doazan et al. 1989; Telting & Kaper 1994), we should study each one of them as exception of the classical rule. This proposition is based on the fact that the spectral classification was made in the optical range and may not apply in the UV spectral range (Walborn 1971; Walborn & Panek 1984; Walborn & Nichols-Bohlin 1987) (see also the SIMBAD database: <http://simbad.u-strasbg.fr/simfid.pl>). This means that the spectral classification in the optical and the UV range are not always in accordance. As a result, some early Be stars could be late Oe stars and we know that it is a common phenomenon to observe high radial velocities of SACs/DACs in Oe stars. However, in the case of Be stars, we do not observe the same phenomenon. This difference in the behavior of density regions in Oe and Be stars is very interesting and requires further investigation. Finally, we should pay attention in the way the radial velocities are calculated. The classical method considered that the whole observed feature corresponds to only one spectral line, meaning that the radial velocity was calculated by the displacement of the deeper point of the observed feature. Considering the SACs idea, the observed feature consists of a number of spectral line components. As a result, the deeper point of the observed feature is only the result of the synthesis of all the SACs. In this case we should calculate the radial velocity of every one of these components.

An emission component is present in the spectra of B0, B2, B2.5, B3, B6, B7, B8 and B9 type stars (Fig. 7). This means that the emission does not appear in the spectra of the middle spectral subtypes of the Be stars (Kondo, Modisette, & Wolf 1975). The radial velocity of the emission component decreases as the rotational velocity increases. The emission component presents positive or negative radial velocities. If one takes into account that negative radial velocities exist, which is not in agreement

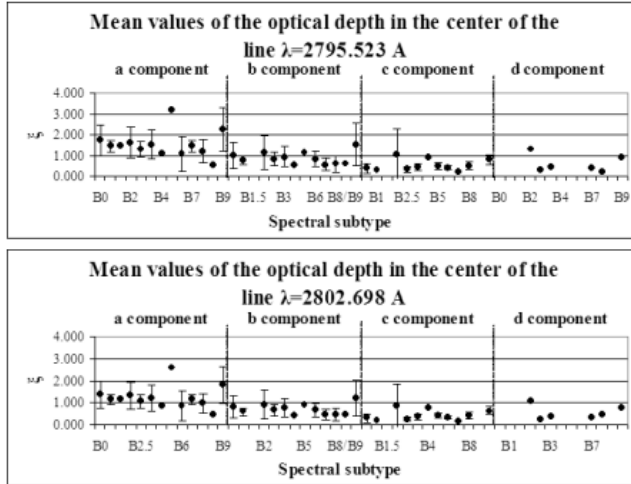


Fig. 9. Mean values of the optical depth ξ in the center of the line for all kinematically separated components of each resonance line, as a function of the spectral subtype.

with the assumption that all emission components are the emission part of P Cygni profiles formed by scattering, one can assume the following. The obtained velocities correspond to the regions where the emission component is created as e.g. strings, blobs, puffs, bubbles. This means that the emission region may approach or move away from the observer and its different position and motion around the star is responsible of whether this value is positive or negative. In Fig. 7 and 8 one can see that, as the rotational velocity increases, the radial velocity decreases, in contrast with the relation of the two velocities of the absorption components. A problem with the emission component is that it is blended with absorption lines of other ions and thus it is difficult to evaluate the rotational and radial velocities. As a result the calculated values present greater statistical error than in the case of the absorption components.

According to criteria described in Danezis et al. (2003), the same components of the two resonance lines should have the same values of rotational and radial velocities and the ratio of the optical depth (ξ) should be the same as the respective ratio of relative intensities. In Fig. 9 we present the mean values of the optical depth (ξ) in the center of the line for all kinematically separated components of each resonance line, as a function of the spectral subtype. As one can see, the value of ξ of the first kinematical region is obviously higher than in the rest three. It tends to decrease from the first to the fourth kinematical region. That, also, may indicate physically separated regions.

5. Conclusions

We applied the method developed in Danezis et al. (2003) and Lyratzi & Danezis (2004) on the Mg II resonance lines of 64 Be stars in order to investigate the kinematical properties of the Mg II resonance lines forming

region. We obtained the rotational and radial velocities which allow us to extract some general physical properties for the Mg II regions of Be stars. Some interesting results inferred from the investigations are the following: (i) the proposed rotation model gives satisfactory results for the Mg II $\lambda\lambda$ 2795.523, 2802.698 Å resonance lines region; (ii) the absorption atmospheric region where the Mg II resonance lines are created presents a complex structure. It tends to be composed by more than one kinematically independent regions (Only four stars present simple structure). We found that the kinematically independent regions rotate with different velocities: 22 km s⁻¹, 41 km s⁻¹, 69 km s⁻¹, 130 km s⁻¹. The respective radial velocities are near zero for all these regions. These calculated values lead us to accept that the Mg II resonance lines of the Be stellar spectra present Satellite Absorption Components. (iii) the rotational velocities of the found independent regions present a uniform fluctuation with the spectral subtype. (iv) the emission lines were detected in the earliest and latest spectral subtypes with the majority of positive radial velocities with several exceptions, i.e. with radial velocities within the range 0 to -87 km s⁻¹, and taking into account that the positive values, if lines are formed by scattering, are not radial velocities.

6. Acknowledgments

This research project is progressing at the University of Athens, Department of Astrophysics, Astronomy and Mechanics, under the financial support of the Special Account for Research Grants, which we thank very much. This work also was supported by Ministry of Science and Environment Protection of Serbia, through the projects Influence of collisional processes on astrophysical plasma line shapes and Astrophysical spectroscopy of extragalactic objects. Finally, we thank the anonymous referee for his/her very useful comments.

Appendix 1. Calculation of the distribution functions L

As we know the distribution function (L) of the absorption coefficient (k_λ) has the same form as the distribution function of each component of the spectral line. This means that we can replace the distribution function of the absorption coefficient L_i , with another expression of the distribution function of each component.

It is also known that Be and Oe stars are rapid rotators. This means that we accept that the main reason of the line broadening is the rotation of the regions that produce each satellite component of the whole observed spectral feature. These rapidly rotating density regions may also present radial motion. For these two reasons we search another expression for the distribution function of the spectral line's components that has as parameters the rotational and radial velocities of the spherical density regions.

For a spherical density region, we assume the following hypotheses: i) The natural broadening of the spectral lines follows the Lorentz distribution; ii) Lambert's sinus law stands for each point of the spherical region; iii) The angular velocity of rotation is constant.

In order to calculate the total radiation, we divide the spherical layer in very thin cylindrical surfaces which are perpendicular to the rotational axis. Lambert's law allows us to consider that the luminosity from each point on the sphere is the same.

On the above cylindrical surfaces we also consider the surface dS . According to Lambert's law, when this surface rotates with an angular velocity ω , its radiation intensity is:

$$dI(\omega) = Q(\omega)dS \cos \theta, \quad (A1)$$

where θ is the angle between the vertical on dS and the line of sight and

$$Q(\omega) = C_1 \frac{\gamma}{(\omega - \omega_k)^2 + \left(\frac{\gamma}{2}\right)^2},$$

C_1 is a constant and γ is the Lorentzian full width at half maximum, which, in the case of the natural broadening, has the value $\gamma \cong 10^8 \text{ Hz}$.

When the surface dS does not rotate, the center of the formed spectral line has the observed wavelength λ_0 , which corresponds to a frequency ν_0 . Thus, we have:

$$\omega_0 = 2\pi\nu_0 = 2\pi \frac{c}{\lambda_0}.$$

When the surface dS rotates with a rotational velocity V_{rot} , the center of the formed line has the wavelength λ_k and in this case we have $\omega_k = \omega_0(1 - z \sin \varphi)$, where $z = \frac{V_{rot}}{c}$.

We also have $\cos \theta \cong \cos \alpha \cos \varphi$. The angles α and φ are shown in Fig. 10.

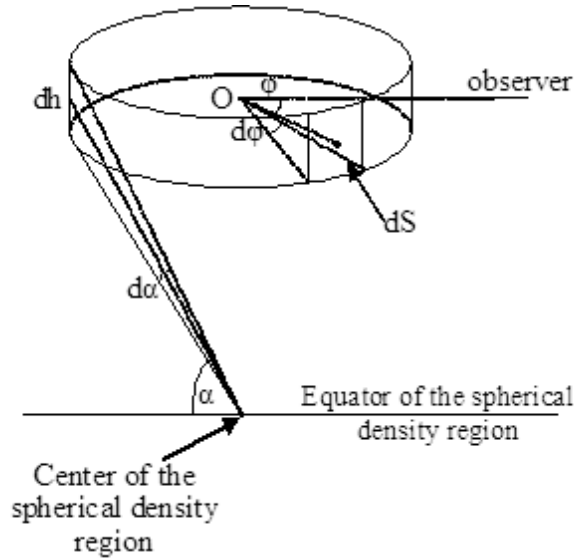


Fig. 10. Elementary ring of the spherical density region.

The surface dS can be written as $dS = r dh d\varphi$, where r is the radius of the cylinder, $d\varphi$ is the angle under which the observer sees dS and dh is the height of dS .

Making the above substitutions in Eq. (A1), we have:

$$dI(\omega) = \frac{C_1 r dh \gamma \cos \alpha \cos \varphi d\varphi}{[\omega - \omega_0(1 - z \sin \varphi)]^2 + \left(\frac{\gamma}{2}\right)^2}$$

Thus, the radiation intensity from the semi cylinder is

$$I(\omega) = \int_{-\pi/2}^{\pi/2} \frac{C_1 r dh \gamma \cos \alpha \cos \varphi d\varphi}{[\omega - \omega_0(1 - z \sin \varphi)]^2 + \left(\frac{\gamma}{2}\right)^2}$$

or

$$I(\omega) = \frac{4C_1 r dh}{\gamma} \int_{-\pi/2}^{\pi/2} \frac{\cos \alpha d \sin \varphi}{\left[\left(\frac{\omega}{\gamma/2} \right) - \left(\frac{\omega_0}{\gamma/2} \right) (1 - z \sin \varphi) \right]^2 + 1}$$

If we take that $\tilde{\omega} = \frac{\omega}{\gamma/2}$, $\tilde{\omega}_0 = \frac{\omega_0}{\gamma/2}$, $x = \sin \varphi$, we have

$$I(\tilde{\omega}) = \frac{4C_1 r \cos \alpha dh}{\gamma} \int_{-1}^1 \frac{dx}{[\tilde{\omega} - \tilde{\omega}_0(1 - zx)]^2 + 1}$$

Taking that $y = \tilde{\omega} - \tilde{\omega}_0(1 - zx)$, the above integral becomes

$$I(\tilde{\omega}) = \frac{4C_1 r \cos \alpha dh}{\gamma \tilde{\omega}_0 z} \int_{\tilde{\omega} - \tilde{\omega}_0(1+z)}^{\tilde{\omega} - \tilde{\omega}_0(1-z)} \frac{dy}{y^2 + 1}.$$

Finally, we have

$$I(\tilde{\omega}) = \left(\frac{4C_1 r \cos \alpha dh}{\gamma} \right) \left(\frac{\arctan[\tilde{\omega} - \tilde{\omega}_0(1 - z)] - \arctan[\tilde{\omega} - \tilde{\omega}_0(1 + z)]}{\tilde{\omega}_0 z} \right). \quad (\text{A2})$$

The above function describes the radiation intensity from a visual semi cylinder with radius r and height dh .

Under the angle $d\alpha$ is seen dh from the center of the spherical region. This cylinder rotates with a rotational velocity $z = \frac{V_{rot}}{c}$ and a constant angular velocity $\tilde{\omega}$.

We consider the function:

$$P(\tilde{\omega}, z) = \frac{\arctan[\tilde{\omega} - \tilde{\omega}_0(1 - z)] - \arctan[\tilde{\omega} - \tilde{\omega}_0(1 + z)]}{\tilde{\omega}_0 z}$$

We study the limit of this function in the case that the density layer does not rotate, i.e. when $z \rightarrow 0$. In such a case:

$$\lim_{z \rightarrow 0} P(\tilde{\omega}, z) = \lim_{z \rightarrow 0} \frac{\arctan[\tilde{\omega} - \tilde{\omega}_0(1 - z)] - \arctan[\tilde{\omega} - \tilde{\omega}_0(1 + z)]}{\tilde{\omega}_0 z}.$$

We apply the De L' Hospital's low and we have:

$$\lim_{z \rightarrow 0} P(\tilde{\omega}, z) = \lim_{z \rightarrow 0} \frac{\frac{d}{dz} \{\arctan[\tilde{\omega} - \tilde{\omega}_0(1 - z)]\} - \frac{d}{dz} \{\arctan[\tilde{\omega} - \tilde{\omega}_0(1 + z)]\}}{\frac{d}{dz} (\tilde{\omega}_0 z)}$$

$$\lim_{z \rightarrow 0} P(\tilde{\omega}, z) = \lim_{z \rightarrow 0} \left[\frac{1}{1 + [\tilde{\omega} - \tilde{\omega}_0(1 - z)]^2} + \frac{1}{1 + [\tilde{\omega} - \tilde{\omega}_0(1 + z)]^2} \right] = \frac{2}{(\tilde{\omega} - \tilde{\omega}_0)^2 + 1}.$$

It is obvious that in the non-rotating case this form corresponds to the Lorentz's distribution for the naturally broadened spectral lines.

In the case when the rotation broadening $|\lambda_1 - \lambda_2|$ (or $|\omega_1 - \omega_2|$) is much larger than the natural broadening (the natural broadening of a spectral line is of an order of $10^{-3} - 10^{-4} \text{ \AA}$), the above function $P(\tilde{\omega}, z)$ presents the form of one quadratic pulsation (see Fig. 11)

For each ω with $\omega_1 < \omega < \omega_2$ the relative shift is $z = \frac{|\Delta\omega|}{\omega_0}$. For the point ω_1 we have $\frac{\omega_0 - \omega_1}{\omega_0} = z$ so that $\omega_1 = \omega_0(1 - z)$. Likewise, for the point ω_2 we have $\omega_2 = \omega_0(1 + z)$. But $\omega = 2\pi\nu = \frac{2\pi c}{\lambda}$. Thus, $\lambda_1 = \frac{\lambda_0}{1 - z}$ and $\lambda_2 = \frac{\lambda_0}{1 + z}$ with $\lambda_1 > \lambda_2$.

This means that $\Delta\lambda_{total} \equiv \lambda_1 - \lambda_2 = \frac{2\lambda_0 z}{1 - z^2}$ and so

$$\lambda_{\min} \equiv \lambda_2 = \lambda_0 - \frac{\Delta\lambda_{total}}{2} = \lambda_0 - \lambda_0 \frac{z}{1 - z^2} \text{ and } \lambda_{\max} \equiv \lambda_1 = \lambda_0 + \frac{\Delta\lambda_{total}}{2} = \lambda_0 + \lambda_0 \frac{z}{1 - z^2}.$$

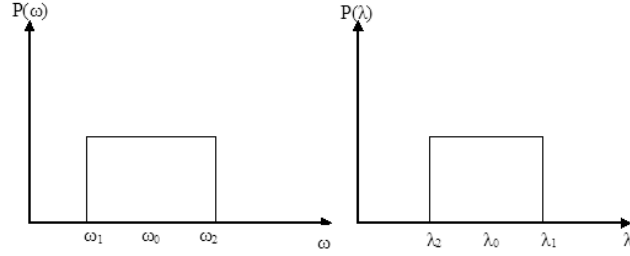


Fig. 11. Quadratic pulsation.

We set $\rho = \lambda_0 \frac{z}{1-z^2}$ and normalize to 1. In this way the function $P(\tilde{\omega}, z)$ could be approximated with the function $f(\lambda)$ where:

$$f(\lambda) = \begin{cases} 1 & |\lambda - \lambda_0| < \rho \\ 0 & \text{otherwise} \end{cases}$$

Now, we assume that the spherical density region rotates with equatorial velocity $z_0 = \frac{V_0}{c}$ (Fig. 12).

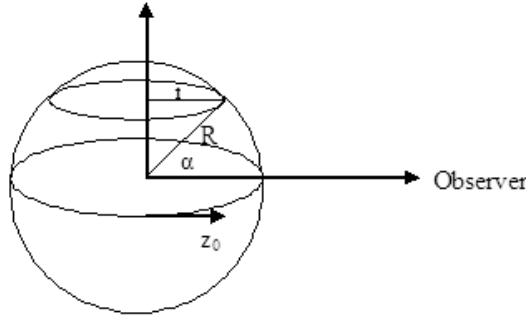


Fig. 12. Rotating spherical density region that produces SACs or DACs.

The points of the circle with radius r rotate with a velocity V_{rot} and for $r = R \cos \alpha$ we take

$$V_{rot} = \omega r = \omega R \cos \alpha.$$

We set $V_0 = \omega R$. Also $\omega = const$. So: $V_{rot} = \frac{V_0}{R} R \cos \alpha = V_0 \cos \alpha$ and $z = z_0 \cos \alpha$. We have also $dh = R d\alpha$ and Eq. (A1) becomes

$$dI(\tilde{\omega}) = \frac{4C_1 R}{\gamma} \cdot \frac{\arctan[\tilde{\omega} - \tilde{\omega}_0(1 - z_0 \cos \alpha)] - \arctan[\tilde{\omega} - \tilde{\omega}_0(1 + z_0 \cos \alpha)]}{\tilde{\omega}_0 z_0 \cos \alpha}.$$

The integral of this equation is

$$I(\tilde{\omega}) = \frac{4C_1 R}{\gamma} \int_{-\pi/2}^{\pi/2} \frac{\arctan[\tilde{\omega} - \tilde{\omega}_0(1 - z_0 \cos \alpha)] - \arctan[\tilde{\omega} - \tilde{\omega}_0(1 + z_0 \cos \alpha)]}{\tilde{\omega}_0 z_0 \cos \alpha} \cos \alpha d\alpha. \quad (\text{A3})$$

When we take into account the function $P(\tilde{\omega}, z)$ the above function becomes

$$I(\tilde{\omega}) = \frac{4C_1 R}{\gamma} \int_{-\pi/2}^{\pi/2} P(\tilde{\omega}, z_0 \cos \alpha) \cos \alpha d\alpha.$$

We approximate $P(\tilde{\omega}, z_0 \cos \alpha)$ with $f(\lambda)$ for and we take the integral for the observation angle $\theta \in [-\theta_0, \theta_0]$ from the equatorial plane.

So we have that

$$I(\tilde{\omega}) \cong I_1 = \frac{4C_1 R}{\gamma} \int_{-\theta_0}^{\theta_0} 1 \cdot \cos \theta d\theta.$$

$$I_1 = \frac{4C_1R}{\gamma} \int_{-\theta_0}^{\theta_0} \cos\theta d\theta = \frac{4C_1R}{\gamma} [\sin\theta]_{-\theta_0}^{\theta_0} = \frac{8C_1R}{\gamma} \sin\theta_0.$$

If we normalize to 1, we have

$$I_1 = \sin\theta_0 = \sqrt{1 - \cos^2\theta_0}.$$

For the angle θ_0 we have

$$|\lambda - \lambda_0| \leq \rho_0 = \frac{\lambda_0 z_0 \cos\theta_0}{1 - z_0^2 \cos^2\theta_0}.$$

For a wavelength λ or for a shift $\Delta\lambda = |\lambda - \lambda_0|$ from the center of the spectral line, the absorbing (or emitting) regions are those with angular distance θ from the equatorial plane, with $|\theta| \leq \theta_0$.

For the equatorial plane we have

$$\Delta\lambda = \frac{\lambda_0 z_0 \cos\theta_0}{1 - z_0^2 \cos^2\theta_0}.$$

From this equation we can calculate the angle θ_0 as follows:

$$\cos\theta_0 = \frac{-\lambda_0 \pm \sqrt{\lambda_0^2 + 4\Delta\lambda^2}}{2\Delta\lambda z_0}.$$

As θ_0 is between $-\pi/2$ and $\pi/2$ we have $\cos\theta_0 \geq 0$ and so

$$\cos\theta_0 = \frac{-\lambda_0 + \sqrt{\lambda_0^2 + 4\Delta\lambda^2}}{2\Delta\lambda z_0}.$$

Thus, the distribution function I_1 takes its final form:

$$I_1 = \sqrt{1 - \cos^2\theta_0} \text{ if } \cos\theta_0 = \frac{-\lambda_0 + \sqrt{\lambda_0^2 + 4\Delta\lambda^2}}{2\Delta\lambda z_0} < 1 \text{ and} \\ I_1 = 0, \text{ otherwise.}$$

It is obvious that the distribution function I_1 is a function of the wavelength (λ). This means that $I_1 = I_1(\lambda)$. This distribution function has the same form as the distribution function of the absorption coefficient L and may replace it (in $e^{-L\xi}$), when the main reason of the line broadening is the rotation. We name it Rotation distribution function.

The spectral line profile, which is formed by a spherical density region, is reproduced by the function $e^{-L\xi}$ by applying the appropriate value of the rotational velocity V_{rot} (from z_0), the radial velocity V_{rad} (from $\frac{V_{rad}}{c} = \frac{\lambda_0 - \lambda_{lab}}{\lambda_{lab}}$) and the optical depth ξ in the center of the line.

References

- Andrillat, Y. 1983, A&AS53, 319
 Andrillat, Y. & Fehrenbach, Ch. 1982, A&AS48, 93
 Bates, B. & Halliwell, D. R. 1986, MNRAS223, 673
 Cidale, L. S. 1998, ApJ502, 824
 Cowley, A., Cowley, C., Jaschek, M. & Jaschek, C. 1969, AJ74, 375
 Cowley, A. 1972, AJ77, 750
 Cranmer, S. R. & Owocki, S. P. 1996, ApJ462, 469
 Cranmer, S. R., Smith, M. A. & Robinson, R. D. 2000, ApJ537, 433
 Dachs, J. 1980, ESA SP-157 139
 Danezis, E. 1984, The nature of Be stars, PhD Thesis (University of Athens)
 Danezis, E. 1987, IAU, Colloq. No 92, Physics of Be Stars (Cambridge University Press)
 Danezis, E., Theodossiou, E. & Laskarides, P. G. 1991, Ap&SS179, 111
 Danezis, E., Nikolaidis, D., Lyratzi, V., Stathopoulou, M., Theodossiou, E., Kosionidis, A., Drakopoulos, C., Christou G. & Koutsouris, P. 2003, Ap&SS284, 1119
 Danezis, E., Popović, L. Č., Lyratzi, E. & Dimitriević, M. S. 2006, 23rd Summer School and International Symposium on the Physics of Ionized Gases, (SPIG 2006), Kopaonik, Serbia
 de Jager, C., Kondo, Y., Hoekstra, R., van der Hucht, K. A., Kamperman, T. M., Lamers, H. J. G. L. M., Modisette, J. L. & Morgan, T. H. 1979, ApJ230, 534
 Doazan, V. 1982, B Stars with and without emission lines (NASA SP-456)
 Doazan, V., Barylak, M., Rusconi, L., Sedmak, G., Thomas, R. N. & Bourdonneau, B. 1989, A&A210, 249
 Doazan, V., Sedmak, G., Barylak, M. & Rusconi, L. 1991, A Be Star Atlas of Far UV and Optical High-Resolution Spectra (ESA SP-1147, Paris: ESA Sci. Publ.)
 Fullerton, A. W., Massa, D. L., Prinja, R. K., Owocki, S. P. & Cranmer, S. R. 1997, A&A327, 699
 Grady, C. A., Sonneborn, G., Chi-chao Wu & Henrichs, H. F. 1987, ApJS65, 673
 Guetter, H. H. 1968, PASP80, 197
 Gurzadyan, G. A. 1975, PASP87, 289
 Herbig, G. H. & Spalding J. Jr 1955, ApJ121, 118
 Henrichs, H. F. 1984, 4th European IUE Conf., ed E. Rolfe, & B. Battrick (ESA SSSP-218) p.43
 Houk N. & Smith-Moore M. 1988, MSS C04, 0
 Houziaux, L. & Andrillat, Y. 1976, IAU Symp. No 70, Be and Shell Stars, ed A. Slettebak (Dordrecht: Reidel) p. 87
 Hutsemékers, D. 1985, A&AS60, 373
 Kaper, L., Henrichs, H. F., Nichols, J. S., Snoek L. C., Volten, H. & Zwarthoed G. A. A. 1996, A&AS116, 257

- Kaper, L. Henrichs, H. G., Fullerton, A. W., Ando, H., Bjorkman, K. S., Gies D. R., Hirata, R., Dambe, E., McDavid, D. & Nichols, J. S. 1997, A&A327, 281
- Kaper, L., Henrichs, H. F., Nichols, J. S. & Telting, J. H. 1999, A&A344, 231
- Kelly, R. L. 1979, Atomic emission lines in the near ultraviolet (NASA, TM 80268)
- Kondo, Y., Modisette, J. L. & Wolf, G. W. 1975, ApJ199, 110
- Kondo, Y., Morgan, T. H. & Modisette, J. L. 1976, ApJ209, 489
- Lamers, H. J. G. L. M., Faraggiana, R. & Burger, M. 1980, A&A82, 48
- Laskarides, P. G., Danezis, E. & Theodossiou, E. 1992, Ap&SS179, 13
- Lesh, J. R. 1968, ApJS17,371
- Lyratzi, E., Danezis, E., Stathopoulou, M., Theodossiou, E., Nikolaidis, D., Drakopoulos, C. & Soulikias, A. 2003, Publ. Astron. Obs. Belgrade 76, 27-42
- Lyratzi, E. & Danezis, E. 2004, AIP Conference Proceedings 740, 458
- Lyratzi, E., Danezis, E., Nikolaidis, D., Popović, L. Č., Dimitrijević, M. S., Theodossiou, E. & Antoniou, A. 2005, MSAIS, 7, 114
- Lyratzi, E., Danezis, E., Antoniou, A., Nikolaidis, D., Popović, L. Č. & Dimitrijević, M. S. 2006, IAUID, 4, 10
- Markova, N. 2000, A&AS144, 391
- Marlborough, J. M., Snow, T. P. & Slettebak, A. 1978, ApJ224, 157
- Moore, Ch. 1968, NBS circ. 488
- Morgan, T. H., Kondo, Y. & Modisette, J. L. 1977, ApJ216, 457
- Morgan, W. W., Code, A. P. & Whitford, A. E. 1955, ApJS2, 41
- Mullan, D. J. 1984a, ApJ283, 303
- Mullan, D. J. 1984b, ApJ284, 769
- Mullan, D. J. 1986, A&A165, 157
- Osawa, K. 1959, ApJ130, 159
- Peters, G.J. 1976, IAU Symp. No 70, Be and Shell Stars, ed A. Slettebak (Dordrecht: Reidel) p.209
- Peton, A. 1974, Space Sci. Rev.30, 481
- Popović, L. Č., Dimitrijević, M. S., Mediavilla, E., Danezis, E., Lyratzi, E., Bon, E., Ilić, D., Jovanović, P., Theodossiou, E. & Dačić, M. 2004, AIP Conference Proceedings 740, p.497
- Prinja, R. K. & Howarth, I. D. 1988, MNRAS233, 123
- Rivinius, Th., Stahl, O., Wolf, B., Kaufer, A., Gang, Th., Gummertsbach, C. A., Jankovics, I., Kovacs, J., Mandel, H., Peitz, J., Szeifert, Th. & Lamers, H. J. G. L. M. 1997, A&A318, 819
- Sahade, J., Brandi, E. & Fontela, J.M. 1984, A&AS56, 17
- Sahade, J. & Brandi, E. 1985, Rev. Mex. Astron. Astrofis. 10, 229
- Slettebak, A. 1954, ApJ119, 146
- Slettebak, A. & Snow, T. P. 1978, ApJL224, L127
- Smith, M. A. 2001, PASP113, 882
- Snow, T.P. 1975, ApJ198, 361
- Snow, T.P., Peters, G.J. & Mathieu, R.D. 1979, ApJS39, 359
- Telting, J. H. & Kaper, L. 1994, A&A284, 515
- Tuthill, P., Monnier, J. & Danchi, W. 1999, Nature398, 487
- Underhill, A. B. 1970, Spectral Line Formation in Steady State Extended Atmospheres, ed H. G. Groth & P. Wellman (Nat. Bureau of Standards, Washington) p.3
- Underhill, A. B. 1975, ApJ199, 691
- Underhill, A. B. & Fahey, R. P. 1984, ApJ280, 712
- Walborn, N. R. 1971, ApJS23, 257
- Walborn, N. R. & Panek, R. J. 1984, PASP280L, 27
- Walborn, N. R. & Nichols-Bohlin, J. 1987, PASP99, 40
- Waldron, W. L., Klein, L. & Altner B. 1992, ASP Conf. Series 22, 181